Helium irradiation effects in polycrystalline Si, silica, and single crystal Si

K. J. Abrams,[1,a)] J. A. Hinks,[2] C. J. Pawley,[1,2] G. Greaves,[1] J. A. van den Berg,[1] D. Eyidi,[3] M. B. Ward,[4] and S. E. Donnelly[2]
[1]*Materials and Physics Research Centre, University of Salford, Salford, United Kingdom*
[2]*School of Computing and Engineering, University of Huddersfield, Huddersfield, United Kingdom*
[3]*Institut Pprime, Université de Poitiers, Poitiers, France*
[4]*Institute for Materials Research, University of Leeds, Leeds, United Kingdom*

(Received 2 September 2011; accepted 23 March 2012; published online 26 April 2012)

Transmission electron microscopy (TEM) has been used to investigate the effects of room temperature 6 keV helium ion irradiation of a thin (≈55 nm thick) tri-layer consisting of polycrystalline Si, silica, and single-crystal Si. The ion irradiation was carried out *in situ* within the TEM under conditions where approximately 24% of the incident ions came to rest in the specimen. This paper reports on the comparative development of irradiation-induced defects (primarily helium bubbles) in the polycrystalline Si and single-crystal Si under ion irradiation and provides direct measurement of a radiation-induced increase in the width of the polycrystalline layer and shrinkage of the silica layer. Analysis using TEM and electron energy-loss spectroscopy has led to the hypothesis that these result from helium-bubble-induced swelling of the silicon and radiation-induced viscoelastic flow processes in the silica under the influence of stresses applied by the swollen Si layers. The silicon and silica layers are sputtered as a result of the helium ion irradiation; however, this is estimated to be a relatively minor effect with swelling and stress-related viscoelastic flow being the dominant mechanisms of dimensional change. © *2012 American Institute of Physics*. [http://dx.doi.org/10.1063/1.4705450]

I. INTRODUCTION

As part of a project aimed at investigating the modification of the mechanical properties of Si by ion implantation, we have explored the effects of helium (He) ion irradiation on polycrystalline (poly-Si), single-crystal Si (c-Si), and silica. This work arose from a project to modify the natural frequency of mechanical resonators, manufactured using Micro-Electro-Mechanical Systems (MEMS) technology, and in particular we were interested in reducing the mean density of the Si by the introduction of significant levels of porosity in the form of He bubbles. Note that we use the term porosity to describe the fraction of the specimen volume occupied by He bubbles (i.e., closed pores containing He).

The implantation of He ions into Si results in the production of bubbles (at concentrations above 3×10^{20} cm^{-3}).[1] Bubble formation and growth are complex phenomena involving point defect production, interaction, mobility, and agglomeration. In general, if bubbles are not observed after implantation then they will not develop during any post-implant thermal treatments.[2] Due to the high permeability of He in Si, bubbles (gas-filled cavities) can evolve into voids (empty-cavities).[3] Such voids can be used to getter impurity metals (via chemisorption to the ultra-clean internal surfaces) enabling lifetime extension of junctions within semiconductor devices and can also be used to tailor impurity distributions (via enhanced diffusion and suppression of secondary defects).[4] Relatively a little work has been carried out on He ion implantation of poly-Si and the effects of grain boundaries on the nucleation and growth of bubbles.

In this work, we report on the effects of high-fluence He ion irradiation on c-Si, poly-Si, and on the sandwiched silica layer. A short, preliminary note on this work was included in recent publication on the Microscope and Ion Accelerator for Materials Investigations (MIAMI) facility.[5] Note that although blistering has been reported on Si surfaces under light-ion irradiation,[6] this does not occur for thin transmission electron microscopy (TEM) foils where stress relief occurs by swelling of the entire specimen. Swelling in He-implanted Si has previously been studied by step-height measurements using atomic force microscopy[1] and ellipsometry[7] with the conclusion that there is a good correlation between bubble volume fraction (bubble porosity) and volume expansion. The use of a layered specimen in the present work enables us to make a direct measurement of (linear) swelling in the poly-Si layer whilst simultaneously monitoring the He bubble morphology. Although our tri-layer geometry is similar to that used by Manuaba *et al.*[8] to study He ion implantation into silica with different stoichiometries, the irradiation direction in the present work is parallel to the layer interfaces (rather than perpendicular) and results in an identical fluence to each layer. It should also be noted that the conclusions of Manuaba *et al.* agree with those of Szakács *et al.*[9] that bubbles do not form in silica due to the high mobility of He in that material.

In a similar TEM study of 17 keV He ion irradiation of a self-supporting thin film, Reutov and Sokhatski[10] reported as-implanted bubble porosity of only 1.6% following implantation to a fluence of 4.5×10^{17} ions cm^{-2}. It should be noted that this figure is an order of magnitude smaller than the results reported here.

a)Electronic mail: k.j.abrams@salford.ac.uk.

II. EXPERIMENTAL DETAILS

The bulk material was prepared at the Scottish Microelectronic Centre at the University of Edinburgh by depositing a 110 ± 3 nm layer of poly-Si onto a 59 ± 1 nm amorphous silica (SiO_2) layer on a {100} Czochralski-grown c-Si wafer by thermal oxidation. The poly-Si was deposited at 570°C by low-pressure chemical vapour deposition in a vertical boat with a deposition rate of 5.5 nm min^{-1} which yielded a mean grain size of ≈20 nm. Cross-sectional specimens were mechanically polished using a tripod system with the minimum possible angle in order to create specimens with the surfaces parallel to each other. Final thinning was performed using 4 keV Ar ions incident at an angle of 4° to the specimen surface in a Gatan Model 691 Precision Ion Polishing System (PIPS). The prepared tri-layer structure and its orientation with respect to the ion and electron beams (the latter being the viewing direction) inside the TEM are illustrated schematically in Fig. 1.

Specimen thickness was determined by tilting an unimplanted specimen to known angles about an axis parallel to the interfaces. This results in clearly visible projections of the interfaces in the recorded images. By measuring the width of this projection and applying the appropriate trigonometric relationship, the sample thickness at the interface can be determined. The thickness at the c-Si/silica interface, for the experiments reported here, was determined using this method to be ≈55 nm. (This method could not be used for implanted specimens in which the bubble contrast obscured the projected interface contrast.) As a result of specimen preparation by tripod polishing and PIPS, the specimens are bevelled in directions both parallel and at right-angles to the interfaces. This thickness variation was measured on similarly, prepared specimens using electron energy-loss spectroscopy (EELS) and was found to be approximately 3 nm of thickness change per 100 nm (which results in a specimen wedge angle of 1.7°) both parallel and at right-angles to the interface. In the area shown in the panels of Fig. 2 (and thus for all the results reported here), the initial specimen thickness was therefore 55 ± 5 nm.

He ion irradiation *in situ* within the TEM was carried out at the MIAMI Facility, details of which have been provided elsewhere[5] but essentially it consists of a JEOL JEM-2000FX TEM—which was operated at 200 keV—coupled to a 100 kV ion accelerator system based on a 0.5–10 kV Colutron ion source capable of producing ion beams of most species. The experiments presented in this paper were performed at room temperature with 6 keV He ions at an ion flux on the order of 10^{13} ions cm^{-2} s^{-1}. Calculations using the Monte-Carlo code SRIM (version 2008.04)[11] indicate that 24% of the incident 6 keV He ions will stop in the 55 nm-thick Si layers. Incident ions are both backscattered and transmitted with 8.4% of incident ions backscattered and the remaining ions transmitted.

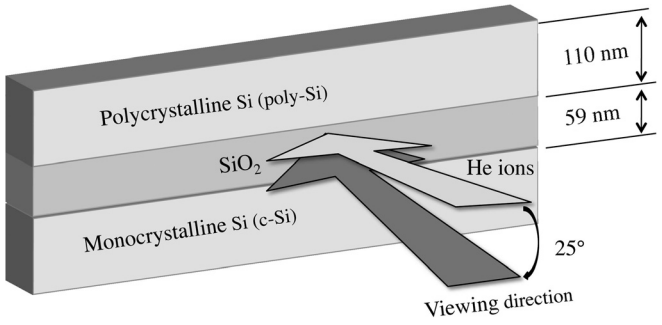

FIG. 1. Schematic illustration of the geometry of the tri-layer used for the *in situ* experiments.

He bubbles were made clearly visible by means of their phase contrast under controlled amounts of objective lens defocus.[12] Images were recorded under conditions in which no Bragg reflection was strongly excited and with the objective lens underfocused by 700–1000 nm. Under these conditions, bubbles appear lighter than the background, and larger bubbles are delineated by a dark fringe.

Images were recorded at fluence steps of approximately 10^{15} ions cm^{-2} using a 1.4 megapixel Gatan ES500W Erlangshen digital camera mounted above the viewing chamber of the TEM. The real space images were post-processed into time-lapse video sequences of the experiments. A video of three experiments can be obtained by email request to the lead author. Note that, in the experiments reported here, the 200 keV electron beam continuously illuminated the specimen; however, our specimen preparation involves having two identical tri-layer specimens glued face-to-face such that two thinned tri-layers are ion irradiated in our experiments. As only one of these is observed by TEM (and thus irradiated with 200 keV electrons), the second serves as a control to determine whether the simultaneous irradiation with electrons during the ion irradiation has any effect on specimen morphology. No differences were seen when this comparison was made, leading to the conclusion that the electron beam caused no perturbation to the effects of the helium irradiation.

EELS experiments to determine oxide stoichiometry were carried out at the Leeds Electron Microscopy and Spectroscopy Centre at the University of Leeds on a Phillips CM200 FEG-TEM operating at 197 kV using a nanofocused beam with a full-width half-maximum (FWHM) diameter of 6 nm. EELS spectra were recorded using a Gatan GIF Model 200.

III. RESULTS

The initial morphology of the tri-layer is shown in Fig. 2(a) in which the 110 nm wide polycrystalline layer can be seen at the top of the image and is separated from the c-Si layer by a 59 nm layer of silica. Note that in order to avoid strong Bragg diffraction in the Si, specimens were generally tilted from "down-zone" alignment. This resulted in a narrow projection of the interface to appear as a band of contrast on either side of the interface (Figs. 2(b)–2(e)). It is this contrast (at larger tilts) that was used to determine specimen thickness.

Following irradiation with 6 keV He ions, a number of changes occur which can be seen in the sequence of images in Fig. 2. These include the development of interstitial-clusters and bubbles, swelling of the Si layers (directly

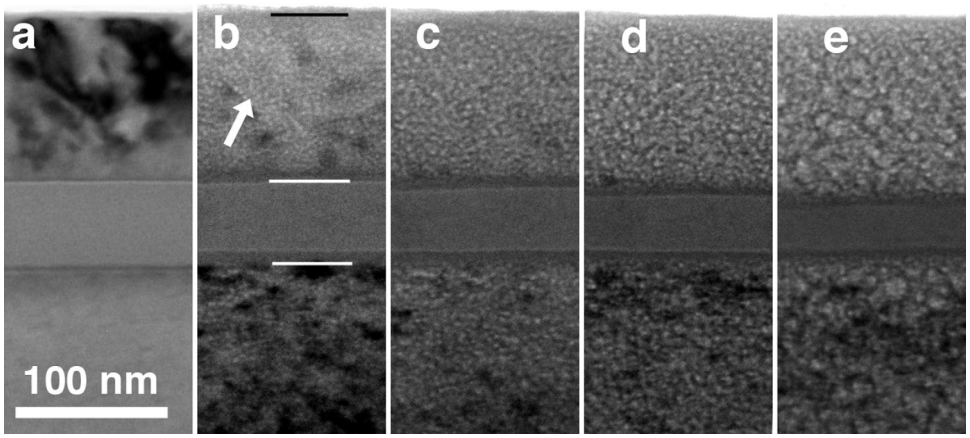

FIG. 2. Bright-field micrographs of the c-Si/silica/poly-Si tri-layer (the poly-Si layer is at the top of the images) following irradiation to nominal fluences of (a) 10^{16}; (b) 10^{17}; (c) 1.5×10^{17}; (d) 2×10^{17}; and (e) 3×10^{17} ions.cm^{-2}. Images were recorded with the objective lens underfocused by approximately 800 nm in order to render small bubbles more clearly visible. Note that the band of contrast on either side of the silica layer in panels (b) to (e) is a projection of the interfaces resulting from a tilt of the specimen through approximately 5° about an axis approximately parallel to the interfaces. In panel (a), the specimen has been tilted by a similar amount about an axis approximately perpendicular to the interfaces. The specimen is tilted in this way in order to avoid exciting strong Bragg reflections in the silicon. Images are aligned at the c-Si/silica interface. The horizontal lines in panel (b) indicate the positions of the interfaces as used in determining the width of the layers. The arrow in panel (b) indicates an alignment of bubbles at a grain boundary.

measurable in one direction in the case of the poly-Si) and a marked shrinkage of the silica layer.

A. Bubble formation

Nanometre-sized He bubbles were first discernible at fluences of approximately 5×10^{16} ions.cm^{-2} in both the poly-Si and c-Si layers and grew in size with increasing fluence; however, the diffraction contrast from interstitial clusters renders it more difficult to observe the bubbles in the c-Si layer. Fig. 2(a) shows the specimen following a fluence of 10^{16} ions.cm^{-2} and is essentially identical to the unirradiated specimen as no radiation-induced contrast is visible at this fluence. (An image of the virgin specimen in the same area is not available due to a change of area following the first fluence steps.) Fig. 2(b) shows the bubble distributions in the two layers following irradiation to a fluence of 10^{17} ions.cm^{-2}. Accurate size measurements of such small bubbles cannot be made but the bubble diameter would generally appear to be less than 1.5 nm.

There appears to be no significant difference in bubble size in the Si layers and grain boundaries in the poly-Si are occasionally seen to be decorated or delineated by bubbles (one example is indicated by the arrow in Fig. 2(b)—although this delineation appears to result from the alignment of the bubbles rather than from their being larger than those within the grains. It should also be noted that, unlike the cases reported for He bubbles in some metals,[13,14] there is not a layer denuded of bubbles in the region of the grain boundaries. Figs. 2(c) and 2(d) show the bubble distributions following implantation to fluences of 1.5×10^{17} and 2×10^{17} ions.cm^{-2}, respectively, and in these images no differences in the bubble distributions can be seen between the poly-Si and c-Si layers. Finally, Fig. 2(e) shows the tri-layer following He implantation to a fluence of 3×10^{17} ions.cm^{-2}. At this fluence, identification of individual bubbles is impossible due to the complex image that results from the significant bubble overlap; however once again, there appears to be no significant difference between the bubble distributions in the two layers. He bubbles do not form in the silica due to the high mobility of He in silica which enables it to diffuse out of the layer.[8,15] Note that we estimate using SRIM (Ref. 11) (but neglecting any diffusive loss of the gas) that, at the highest fluences, the silicon layers may contain up to 26 at. % helium.

B. Development of interstitial clusters

The implantation of He ions into c-Si at room temperature leads to the formation of interstitial clusters with no clear crystallographic features, i.e., the clusters have an approximately spherically symmetrical strain field. These are visible in bright-field TEM in all orientations. Due to the fact that these defects are made visible by the interaction of the electron beam with their strain field (whose extent is much larger than the cluster itself), they are generally visible in TEM at fluences lower than those at which bubbles are visible.

Interstitial clusters are clearly seen in our *in situ* experiments as small black patches of contrast in the c-Si at the bottom of Fig. 2. However in the poly-Si layer, the interstitial clusters generally occur only in the largest grains and inspection of the time-lapse video of the experiments shows that in much of the polycrystalline layer these defects are never observed. For many grains, the boundary is poorly delineated in the individual TEM images, but inspection of sets of images indicates that interstitial clusters are visible in grains with a linear dimension larger than about 50 nm and are not observed in grains smaller than 30 nm. This is shown more clearly in Fig. 3 where interstitial cluster formation is not observed in the area delineated by a continuous white line but interstitial clusters did develop in the area delineated by a dotted line.

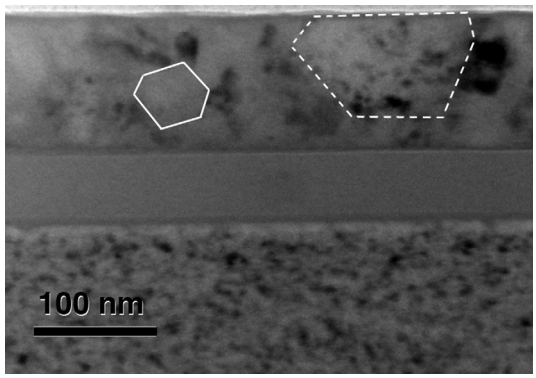

FIG. 3. Bright-field micrograph of interstitial clusters in c-Si (bottom of the image) and poly-Si (top of the image) following irradiation with 6 keV He ions to a fluence of 4.6×10^{16} ions.cm^{-2}. The white lines indicate grain boundaries, the dotted-boundary indicates a grain in which contrast from interstitial clusters is observed, and the continuous boundary indicates a grain in which contrast from interstitial clusters is not observed.

C. Expansion of the Si layers and shrinkage of the silica layer

Larger scale changes are also visible in Fig. 2. In particular, changes to the width of the poly-Si and silica layers are clearly taking place as the fluence is increased—with the poly-Si layer increasing, and the silica layer decreasing, in width. Fig. 4 shows a plot of the width of these two layers as a function of fluence. The poly-Si layer increases from an initial value of 110 ± 3 nm to a final value of 124 ± 3 nm representing a linear increase of 13%.

Shrinkage of the silica layer is observed as shown in the micrographs in Fig. 2 and in the plot in Fig. 4. The shrinkage, after a fluence of 3×10^{17} ions.cm^{-2}, is 26 nm, or 44% of the original layer width. To determine whether the reduction in width of the oxide layer was accompanied by changes in the oxide stoichiometry, *ex situ* EELS measurements were carried out on the centre of the silica layer of both a virgin specimen and a specimen irradiated with a He ion fluence of 2×10^{17} ions.cm^{-2}. EELS spectra were recorded with a range of energy losses from approximately 80 eV to 590 eV (1024 channels at 0.5 eV per channel). The spectra were taken from areas of similar thickness in both specimens, approximately 0.28 λ (where λ is the mean free path for inelastic energy losses in the specimen and thus provides a relative measure of thickness of the two samples). Note that it is expected that the stoichiometry of the implanted specimen was fully preserved on exposure to air during transfer of the specimen between electron microscopes as the diffusivity of oxygen through silica is known to be extremely low at room temperature.[15]

Following background removal (power-law fit) before the Si $L_{2,3}$ and O K-edges, O to Si atomic ratios were calculated using standard quantification procedures and Hartree-Slater cross-sections[16] with an energy integration window at each edge of 50 eV. These measurements yielded nominal values of 2.12 ± 0.30 for the O:Si atomic ratio in the unirradiated oxide and 2.18 ± 0.31 in the irradiated specimen. Therefore, within the experimental errors, this indicates that the stoichiometry of the oxide is unchanged by the He ion irradiation; a conclusion supported by the comparison of the Si $L_{2,3}$ and O K-ELNES (energy loss near-edge spectra) from the two specimens (see Fig. 5) in which identical peak structures (typical of silica) were observed. Note that the irradiated specimen used for the EELS measurements exhibited a reduction of the oxide layer width of approximately 21%.

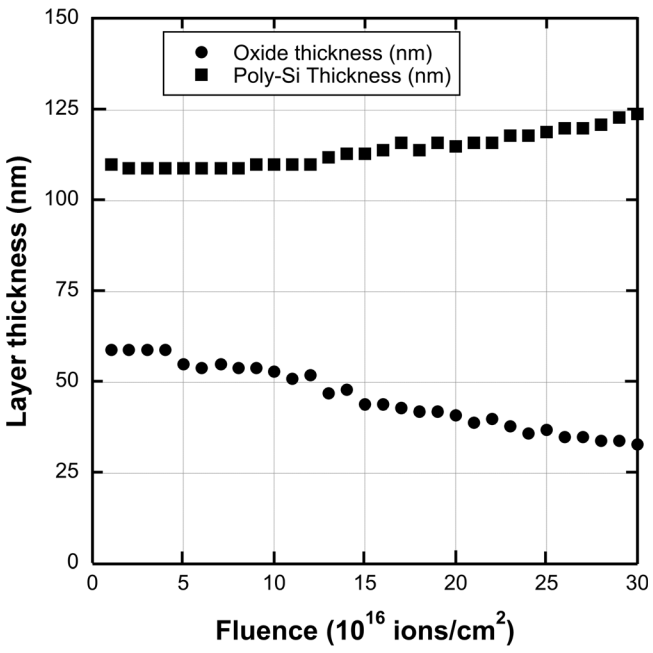

FIG. 4. Plot of the change in thickness of silica and poly-Si layers as a function of He ion fluence.

IV. DISCUSSION

During He ion irradiation, interstitial clusters form throughout the c-Si but rarely occur in the poly-Si. Specifically, interstitial clusters only form in grains that are typically larger than 50 nm. An explanation for this observation almost certainly lies in the competition, within a given grain, between the formation of stable interstitial clusters and the

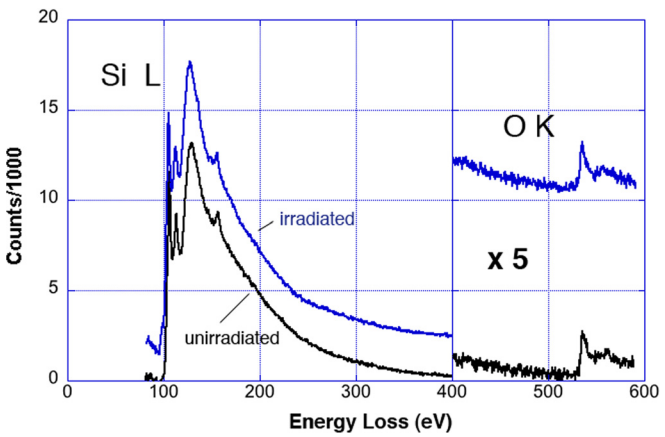

FIG. 5. EELS spectra from the oxide layer in an unirradiated specimen (bottom spectrum) and in a specimen irradiated with 6 keV He ions to a fluence of 2×10^{17} ions.cm^{-2} (top spectrum, blue). Power-law background has been removed in both cases. Note that the spectrum from the irradiated specimen has been vertically offset by 2000 counts for clarity. The electron energy was 197 keV, and the beam spot size was 6 nm FWHM.

trapping of interstitials at grain boundaries; the presence of a nearby grain boundary thus serving greatly to reduce the number of interstitial clusters that form within the grain. This difference in behaviour between the two materials, however, has little or no influence on the nucleation and growth of He bubbles as these processes appear identical in small grains, in larger grains, and in c-Si. In He-irradiated Si, the "primary" process is thus the agglomeration of He atoms and vacancies; the latter thus not contributing to Frenkel pair recombinations that would otherwise take place. The resulting excess interstitials are either absorbed by grain boundaries in poly-Si or form interstitial clusters in c-Si—but their behaviour does not significantly influence bubble nucleation and growth.

Turning to the observed swelling: although only the changes in one dimension in the poly-Si layer can be measured, it should be noted that the layer will also expand, to differing degrees, in the other two dimensions. Expansion in the measured direction is completely unconstrained; in the direction "out of the page" in Fig. 2 it is constrained only at the interface with the silica; and in the third orthogonal direction (along the line of the interface) expansion is both constrained at the interface and to some extent may be constrained by the thicker material at some distance from the imaged area due to the wedge-shaped nature of the specimen (thicker towards the right in Fig. 2). Similar considerations also apply for the c-Si with the addition of constraint due to the wedge-shaped nature of the specimen (thicker towards the bottom in Fig. 2).

For a completely unconstrained layer, a 13% linear increase in each of the three linear dimensions would imply a volume swelling of 44%. On the assumption that the swelling results primarily from the volume of the interstitials displaced from the bubbles (i.e., that there is a negligible contribution from elastic distortion), the corresponding porosity (defined as the bubble volume fraction) would be approximately 31%. The possible ranges of swelling and porosity from these observations thus lie in the ranges between 13%–44% and 12%–31%, respectively. However, the behaviour of the silica layer under irradiation (discussed below) indicates that it is likely to provide minimal constraint to the expansion of the Si layers—in which case the volume swelling and porosity values will lie at the higher end of these ranges.

The measurements on the silica layer show that it shrinks considerably under He ion irradiation but that there is no modification to the stoichiometry. There is a considerable body of literature on the effects of ion irradiation on silica—albeit generally with ions of much higher energies (MeV).[17,18] As a result of work by Brongersma[17] and Snoeks and Polman,[18] it is well established that silica subjected to mechanical stress and under ion irradiation undergoes viscoelastic flow so as to reduce the applied stress to zero. The dimensional changes to the silica layer in the current experiments can be explained in the following manner: the bubble growth in the poly-Si and c-Si layers on either side of the silica layer causes a swelling that applies stress along two dimensions at the interface. If the viscoelastic flow processes reported to occur at MeV ion energies also operate at the much-lower ion-energies used in the present experiments then, in order to reduce the stress to zero, the silica layer must follow the swelling in both Si layers by expanding to match the area at the interfaces. Assuming constant volume and density, the width of the oxide layer will decrease in the unconstrained orthogonal direction, giving rise to shrinkage to compensate for the increase in area. On this basis, a linear Si swelling of 13% would imply an areal swelling of 28% and this areal increase in the oxide layer would be compensated for by shrinkage of 28% in the observed oxide layer width. This is somewhat less than the observed value of 44%.

For He fluences as high as 3×10^{17} ions.cm^{-2}, it is likely that some significant sputtering of Si and silica will have taken place. For 6 keV He on Si, a sputtering yield of 0.15 has been reported.[19] For 6 keV He on silica, we have not found experimental values in the literature; however, the Monte-Carlo code SRIM (Ref. 11) gives values similar to those as for He on Si (0.2 atoms per ion). A sputtering yield in the range of 0.15–0.2 would result in the reduction of the tri-layer thickness by 9–12 nm over the course of the experiment. A uniform sputter-induced reduction of the thickness of the Si and silica layers would leave the conclusions above regarding swelling unchanged. However, preferential sputtering of the silica would lead to a reduction in the silica layer volume and give rise to additional shrinkage of the layer width from viscoelastic flow. The observed 44% reduction in the silica layer width may thus result from a combination of stress induced by the swollen Si layers, viscoelastic flow, and preferential sputtering—all due to the irradiation with the 6 keV He ions.

V. CONCLUSIONS

Investigation of the effects of 6 keV He ion irradiation to high fluences and at room temperature of a tri-layer specimen consisting of c-Si, silica, and poly-Si has yielded a number of findings:

(1) Interstitial clusters, always observed to form in the c-Si, are only seen in the largest grains in the poly-Si leading to the conclusion that the proximity of a grain boundary leads to the trapping of interstitials, which are thus not able to agglomerate into clusters;
(2) No significant difference was seen in bubble behaviour in the poly-Si and c-Si layers (despite the interstitial clusters' observations discussed above). This points to bubble formation being the dominant process with the fate of the interstitials (which cannot recombine with vacancies as these are trapped in the growing bubble nuclei) having a little or no effect on bubble behaviour;
(3) Volume swelling in the Si layers potentially as high as 44% is inferred for high-fluence implantation with 6 keV He ions. This yields a corresponding (closed pore) He-bubble porosity of up to 31%; and
(4) The silica layer has been observed to shrink significantly under He ion irradiation. We attribute this to ion-bombardment-induced viscoelastic flow processes as previously observed to operate for high-energy ion irradiation. The viscoelastic flow takes place under the

action of stress applied by the swollen Si layers and may be augmented by preferential sputtering of the silica.

ACKNOWLEDGMENTS

The authors wish to thank Professor Rik Brydson of the University of Leeds for useful discussion of the EELS measurements and Dr. Les Haworth and Dr. Jon Terry of the University of Edinburgh for providing the c-Si/silica/poly-Si wafer. We acknowledge the UK Engineering and Physical Sciences Research Council (EPSRC) for provision of the funding (Grant No. EP/E017266/1) that enabled the development of the MIAMI facility used for this work and for access to the Leeds EPSRC Nanoscience and Nanotechnology Equipment Facility (Grant No. EP/F056311/1).

[1]V. Raineri, S. Coffa, E. Szilágyi, J. Gyulai, and E. Rimini, Phys. Rev. B **61**, 937 (2000).
[2]V. M. Vishnyakov, S. E. Donnelly, and G. Carter, J. Appl. Phys. **94**, 238 (2003).
[3]C. C. Griffioen, J. H. Evans, P. C. De Jong, and A.van Veen, Nucl. Instrum. Methods Phys. Res. B **27**, 417 (1987).
[4]V. Raineri, M. Saggio, and E. Rimini, J. Mater. Res. **15**, 1449 (2000).
[5]J. A. Hinks, S. E. Donnelly, and J. A. van den Berg, J. Vac. Sci. Technol. A **29**, 021003 (2011).
[6]A. Giguère, J. Beerens, and B. Terreault, Nanotechnology **17**, 600 (2006).
[7]W. Fukarek and J. R. Kaschny, J. Appl. Phys. **86**, 4160 (1999).
[8]A. Manuaba, F. Pászti, A. R. Ramos, N. Q. Khánh, B. Pécz, Z. Zolnai, A. Tunyogi, and E. Szilágyi, Nucl. Instrum. Methods. Phys. Res. B **249**, 150 (2006).
[9]G. Szakács, E. Szilágyi, F. Pászti, and E. Kótai, Nucl. Instrum. Methods. Phys. Res. B **266**, 1382 (2008).
[10]V. F. Reutov and A. S. Sokhatskiĭ, Tech. Phys. **48**, 68 (2003).
[11]J. F. Ziegler, M. D. Ziegler, and J. P. Biersack, Nucl. Instrum. Methods Phys. Res. B **268**, 1818 (2010).
[12]M. Rühle and M. Wilkens, Cryst. Lattice Defects **6**, 129 (1975).
[13]W. Kesternich, D. Schwahn, and H. Ullmaier, Scr. Metall. Mater. **18**, 1011 (1984).
[14]S. J. Zinkle and K. Farrell, J. Nucl Mater. **168**, 262 (1989).
[15]M. A. Lamkin, F. L. Riley, and R. J. Fordham, J. Eur. Ceram. Soc. **10**, 347 (1992).
[16]R. F. Egerton, *Electron Energy-Loss Spectroscopy in the Electron Microscope* (Plenum, New York, London, 1986).
[17]M. L. Brongersma, E. Snoeks, and A. Polman, Appl. Phys. Lett. **71**, 1628 (1997).
[18]E. Snoeks and A. Polman, Appl. Phys. Lett. **65**, 2487 (1994).
[19]H. H. Anderson and H. L. Bay, Top. Appl. Phys. **47**, 145 (1981).